BMC Genomics

RESEARCH

Open Access

The molecular anatomy of cashmere goat hair follicle during cytodifferentiation stage

Minghao Li[1], Xuxu Hao[1], Zixi Cheng[2], Jiamian Du[1], Xinmiao Wang[1], Niu Wang[1], Tongtong Zhang[1], Zhenyu Zhong[1] and Xin Wang[1*]

Abstract

Background Cashmere, named as "soft gold", derives from the secondary hair follicles (SHFs) of cashmere goat which is vital to Northwest China's economy. The cytodifferentiation stage (E120), mirroring the complete hair follicle (HF) structure of adult goats and marking a critical phase in SHF development. Therefore, this study aims to enhance the understanding of SHF development and its impact on fiber quality, informing breeding strategies.

Results From the scRNA-seq data analysis, the intricate processes and transcriptional dynamics of inner layer cell differentiation of HFs were unveiled in this study. we identified nine cell populations during cytodifferentiation and key structures such as the hair shaft and inner root sheath. And we discovered three main inner layer lineages and seven subpopulations, clarifying their roles in specialization and signaling. Pseudotime mapping analysis showed cell evolution from early stage to mature stages marked by unique gene expressions, and the intermediate stage on the differentiation of each lineage was revealed. The identification and spatial localization of specific transcription factors, such as GATA3, LEF1 and PRDM1, as well as keratin genes highlight regulatory pathways involved in HF development, which was further validated by immunofluorescence. These findings suggested the potential strategies to improve fiber quality, and the discovery of diverse cell types and their developmental molecular mechanisms, particularly in this species-specific context, offered a nuanced view of the regulatory mechanisms driving HF development in cashmere goats.

Conclusion Overall, these findings provide a systematic molecular atlas of skin, defining three major branches and cell states of inner layer cells of HF, and determining how the branch-specific transcription factors, keratins, and signals coordinate HF morphogenesis during cytodifferentiation stage. This research not only advances skin tissue research in goats but also holds broader implications for the understanding of HF regeneration and development across various species.

Keywords Cashmere goat, Cellular heterogeneity, Developmental trajectory, Cytodifferentiation stage

*Correspondence:
Xin Wang
xinwang5@nwsuaf.edu.cn
[1]Key Laboratory of Animal Genetics, Breeding and Reproduction of Shaanxi Province, College of Animal Science and Technology, Northwest A&F University, Yangling 712100, China
[2]School of Electronic Science & Engineering, Southeast University, Nanjing, Jiangsu 210096, China

Introduction

The Shaanbei white cashmere goat, renowned for its diverse animal products such as meat and luxurious cashmere, is pivotal to the economy of Northwest China [1]. Its undercoat, termed "soft gold", is especially valued for its luxury. Cashmere stems from the secondary hair follicles (SHFs) of cashmere goat, whose morphogenesis critically influences both the quantity and quality of fiber [2, 3]. Therefore, understanding the follicular morphogenesis of Shaanbei white cashmere goats is essential for the breeding programs targeting cashmere fiber traits.

HF morphogenesis involves the coordinated development of various epithelial and mesenchymal cells and exhibits asynchronous development among different HF types during embryonic growth [4, 5]. Conventional bulk RNA-seq is limited in addressing cell heterogeneity. The advent of single cell RNA sequencing (scRNA-seq) technology provides unprecedented opportunities to identify diverse cell types during HF development, thereby revealing cell-specific identities and developmental states. In goats, the application of scRNA-seq technology has advanced skin tissue research, enabling the identification of 13 cell types, including two types of dermal papilla cells (DPCs), four stem cells, and three sheaths [6]. Pioneering researchers have elucidated the molecular landscape of different lineages during follicle morphogenesis and the heterogeneity of DP in various HFs [7]. In goats, the groundbreaking study of scRNA-seq outlined a DP cell lineage differentiation trajectory, enhancing our understanding of gene functions, signaling pathways, and biological roles in cell fate determination during HF regeneration [8]. Despite these advancements, the challenges remain in fully comprehending the diversity of skin cells.

The mature HF structure, comprising concentric circles of epithelial cells forming the hair shaft and inner root sheath, raises critical questions about hair growth regulation during HF morphogenesis and cellular identity shifts within HF's hierarchical structure. HF morphogenesis during goat embryo period encompasses three stages [9]: induction, organogenesis, and cytodifferentiation (around embryonic day 115; E115), the latter resembling the complete HF structure of adult goats. The cytodifferentiation stage, containing primary hair follicle (PHF) and SHF, serves as an excellent model for studying HF morphogenesis. In mice, previous studies have explored the fate commitment of matrix precursor cells and lineage differentiation into hair shaft (HS) and inner root sheath (IRS) cells during the cytodifferentiation stage [10], and extensive transcriptomic characterization of skin in anagen and telogen phases have been revealed using scRNA-seq [11].

Despite HS and IRS cells influence the characteristics of cashmere, the various cell types and its subgroups, as well as the molecular mechanisms underlying their development remain poorly understood, partly due to species-specific challenges. Therefore, in this study, we utilized scRNA-seq and immunofluorescence (IF) techniques to systematically investigate the specialized processes and spatial dynamics of inner layer cells in HF during the cytodifferentiation stage. We would present the transcriptional landscape of HF inner layer cells in Shaanbei white cashmere goats using the Monocle algorithm, offering valuable insights for future goat breeding programs focused on cashmere traits.

Results

Identification of different cell types in cytodifferentiation goat skin

To comprehensively explore the molecular characteristics of cell composition and significant cell fate transformations during cytodifferentiation stage of HF, we investigated the dorsolateral skin of Shaanbei white Cashmere Goat using the procedure outlined in Fig. 1A. Following meticulous quality control, a total of 4,995 cells were proceeded to downstream analysis, where over 15,000 genes were detected (Fig. S1). The dimensionality reduction analysis of scRNA-seq dataset resulted in 17 clusters with distinct molecular characteristics using the Uniform Manifold Approximation and Projection (UMAP) algorithm (Fig. 1B).

By examining the expression of cluster-specific genes, nine distinct populations were identified in the cytodifferentiation stage based on their marker gene expressions (Fig. S2). Notably, clusters 0, 5, 6, 10, and 11 exhibited elevated levels of the cortex/cuticle (CX) markers *SELENBP1* and *HEPHL1* [11], leading to their designation as the CX population. And a total of nine cell types were categorized from the downstream analysis, including CX, namely transient amplifying cells (TAC; DCN^{hi}, SHH^{hi}) [12], pricytes ($TBX2^{hi}$; $ABCC9^{hi}$) [11], out root sheath (ORS; $SOX9^{hi}$, $KRT5^{hi}$) [13], medulla (ME; $ALDH1A3^{hi}$, $KRT23^{hi}$) [11], inner root sheath (IRS; $GATA3^{hi}$, $KRT25^{hi}$) [14], immune cells ($FCER1A^{hi,}RGS1^{hi}$) [13], endothelial cells ($PLVAP^{hi}$, $PECAM1^{hi}$) [15], dermal papilla (DP; $SOX2^{hi}$, $FGFR1^{hi}$) [16] and CX (Fig. 1C, S2A and S2B). To enhance the differentiation and classification of cell types during the cytodifferentiation stage, we utilized a bubble map to illustrate the expression of more specific marker genes in different cell populations, confirming the reliability of cell type classification (Fig. 1D). Furthermore, to gain the insights into skin composition during cell formation, we analyzed the distribution of the nine populations in the single-cell dataset and ranked them according their proportions. The rankings were CX (1930, 38.64%), IRS (854, 17.10%), ME (849, 17.00%), TAC (808, 16.18%), endothelial cells (233, 4.66%), ORS (138, 2.76%), DP (137, 2.74%), pericytes (28, 0.56%), and

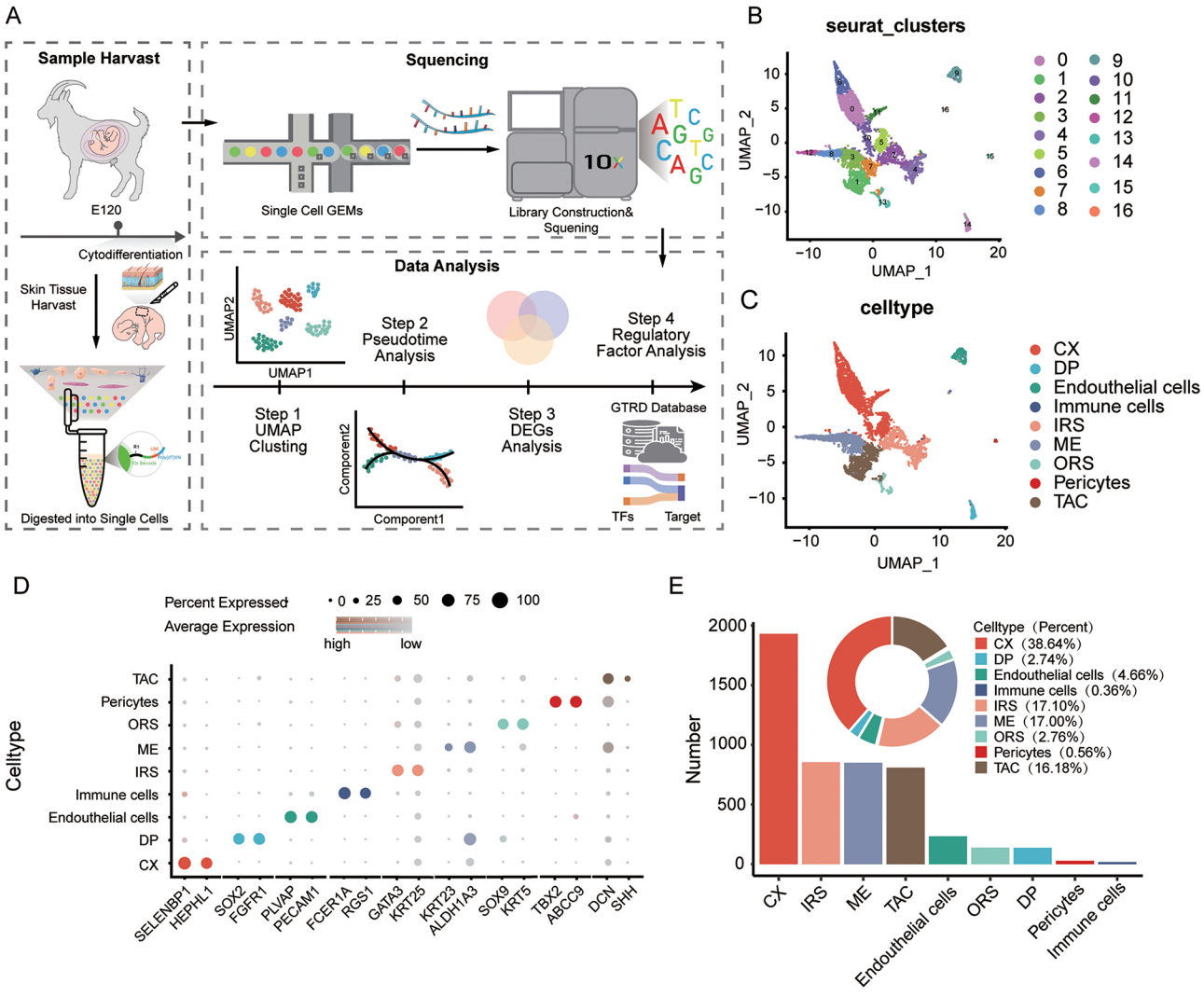

Fig. 1 Comprehensive single-cell transcriptomic atlas of skin during cytodifferentiation stages in hair follicle morphogenesis. **A** Experimental workflow overview. **B** UMAP visualization of all cells ($n = 4,995$) from the main dataset, colored according to primary clusters. **C** UMAP visualization of all cells, colored by principal cell types. **D** Dot plot showing representative marker genes for various cell types. Intensity of color denotes expression level, and dot size indicates the percentage of positive cells (counts > 0). **E** Bar graph and pie chart depicting the count and proportion of different cell types, with each type's percentage in parentheses. Coloring is based on cell type, including Inner Root Sheath (IRS), Cortex/Cuticle (CX), and Medulla (ME)

immune cells (18, 0.36%) (Fig. 1E). The statistical analysis revealed that the ME, IRS, CX, and TAC populations collectively contributed significantly, representing 88.92% of the dataset. In summary, in line with prior research, ME, IRS and CX populations were categorized as epidermal cell lineages, identified as inner layer cells, and prominently featured in the dataset, aligning with the understanding that the CX predominantly constituted the volume of HF morphological structure [11]. Intriguingly, the cell cycle scores revealed a comparable distribution of ME, IRS, and CX cells across G1 phase to those across G2/M and S phases (Fig. S1H). The coexistence of the two subpopulations with distinct proliferative characteristics within the inner layer cells rendered them a compelling model for unraveling the intricacies of HF morphogenesis in cashmere goats.

High-resolution analysis in inner layer cells

In order to dissect the process of HF morphogenesis during cytodifferentiation, we analyzed the correlations among the nine major cell populations using the Pearson correlation coefficient algorithm. The results revealed a high correlation among the IRS, CX, ME, and TAC cell types, all belonging to the epidermal lineage of hair follicle. Specifically, the correlation coefficients exceeding 0.9 among these four populations, referred to as inner layer cells, were closely positioned in the correlation matrix (Fig. 2A). Focusing on the inner layer cells, the inner cell lineage was extracted (TAC, IRS, CX, and

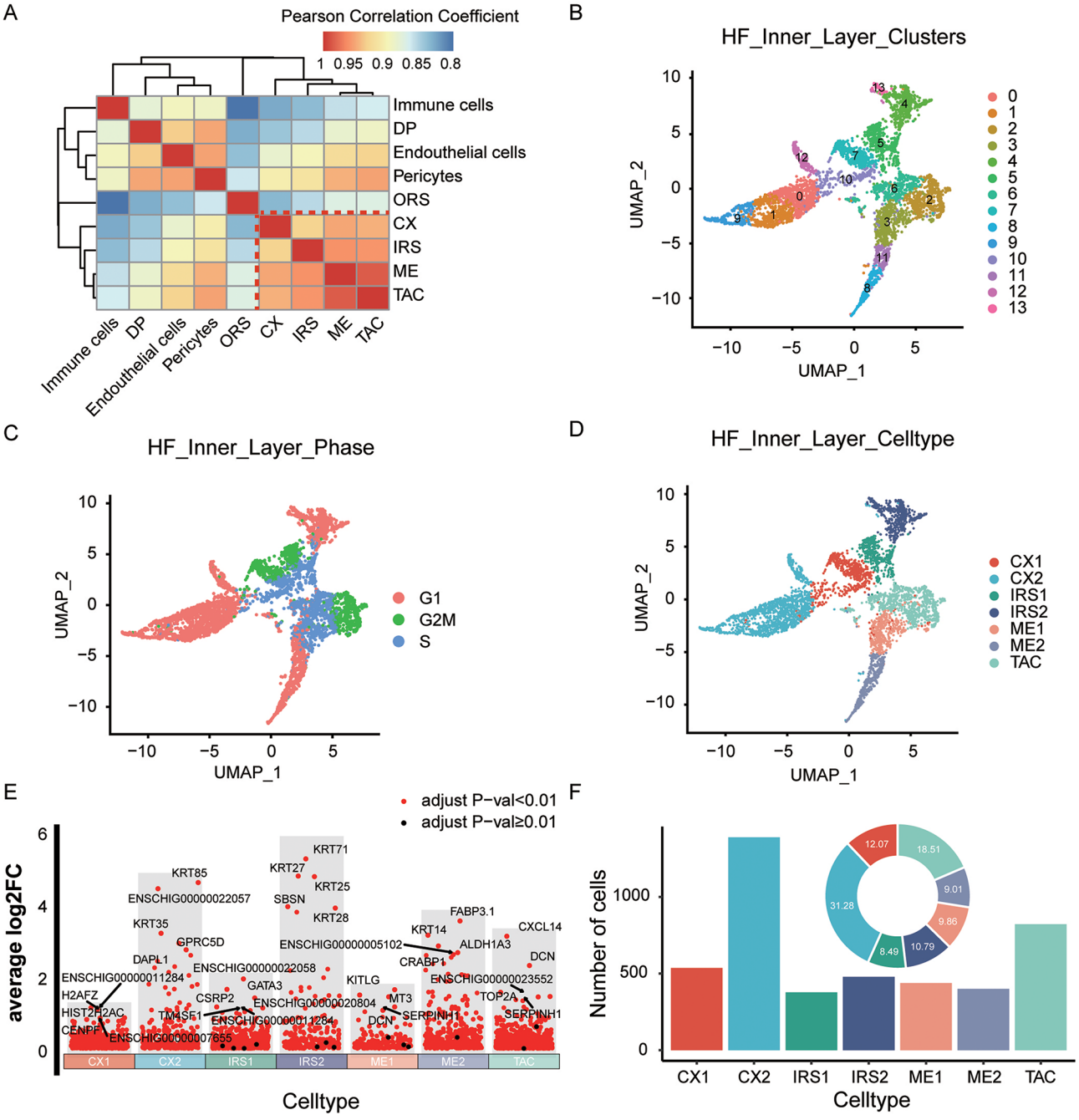

Fig. 2 Principal inner layer cell types in HFs. **A** Heatmap of cell-type Pearson correlation coefficients, highlighting areas of high correlation (red dashed box). UMAP visualizations of inner layer HF cells, colored according to main clusters (**B**), cell cycle stages (**C**), and cell types (**D**), respectively. **E** Volcano plot of top expressed genes in seven inner layer subgroups, highlighting the five most significantly altered genes in each. Red dots indicate genes with an adjusted *P-value* < 0.01; black dots indicate those with an adjusted *P-value* ≥ 0.01. **F**: Bar graph and pie chart showing the count and proportion of different cell subtypes, colored by cell subtype

ME) from the nine main cell populations, conducted a dimensionality reduction analysis, and robustly segregated into 14 clusters displaying a branching topology (Fig. 2B). Contrasting with IRS, ME and CX, the cell cycle score demonstrated that over 90% of TAC cells were in the G2/M and S phases, signifying a population characterized by vigorous proliferation, the multi-branch topology of TAC cells toward IRS, ME, and CX lineages was also supported by a transformation from proliferative to post-mitosis cellular identities of cells within each branch (Fig. 2C and S1H). Intrigued by the intricate peculiarity of the three main cell types, comprising two

mixed but transcriptionally distinct inner cell subtypes and representing early or mature stages of the differentiation process, we delved deeper into their characterization. Although not as exhaustive as studies in other species [17, 18], we followed inner cell markers to identify seven subpopulations (Figs. S3A, S3B, and S3D), the UMAP clusters depicted a multi-branch topology, commencing with the intensely proliferative TAC populations and differentiating through the proliferative subpopulations co-expressing both cell-type-specific and proliferative markers (CX1, ME1, and IRS1); the final destination is reached at the post-mitotic and more differentiated state subtypes (CX2, ME2 and IRS2) (Fig. 2D). Pearson correlation coefficient clustering results demonstrated hierarchical clustering of TAC, CX1, ME1, and IRS1 with high correlation coefficients, likely associated with the vigorous cell proliferation stage (Fig. S3C). Additionally, we presented the highly variable genes of each subpopulation, revealing elevated expression of keratin genes *KRT85*, *KRT14*, and *KRT71* in CX2, ME2, and IRS2, while other subpopulations exhibited high expression levels of cell proliferation-related genes, such as *CENPF* and *TOP2A*, as expected (Fig. 2E and S3B). In sum, we identified seven populations with inner layer cells transcriptional properties and illustrated the composition of hair follicles (Fig. 2F).

Recapitulating developmental trajectories in HF inner lineage branches

Having identified the inner layer cell populations, we next sought to reveal the process of internal cell differentiation for a deeper understanding of each subgroup, which is depicted through a pseudotime developmental trajectory using Monocle (Fig. 3A). The pseudotime trajectory traced a path from the transcriptionally uncommitted proliferative cells (State 2), through the early state cells which co-expressing proliferative and lineage-specific markers (State 3), ending at mature state populations (States 1, 4, and 5). These final states were characterized by high expression levels of lineage-specific markers and were post-mitotic (Figs. 2E and 3A and B). Specifically, the inner layer cells were organized according to the cell types—mature stage cell subgroups ME2, CX2, and IRS2 were in States 1, 4, and 5, respectively; the TAC cell subgroup spaned State 2 and State 1. ME1, CX1, and IRS1 cell types were found where ME2, CX2, and IRS2 types were, with some exclusively at the starting point of pseudotime (State 2) (Fig. 3A and B).

This subgroup cell distribution and cell cycle score information verified the accuracy of pseudotime differentiation trajectory used in this study, endorsing our inner layer cell atlas and supports previous deductions. Subsequently, we generated a heatmap for the top 300 differential genes, exhibiting approximately four patterns of expression (Fig. 3C). The representative genes were selected for display. For cluster 1, *SELENBP1*, *HEPHL1*, and *KRT35* were CX markers; *S100A8* from cluster 3 was an ME marker and *DCN*, from cluster 4, denoted a TAC marker. GATA3 is an IRS transcription factor, with HOXC13 and LEF1 as hair shaft transcription factors. The k-means clustering differential gene heatmap revealed that during the differentiation journey from TAC cells to ME2, CX2, and IRS2, keratin genes such as *KRT35*, *KRT85*, and *KRT84* were upregulated, while genes primarily expressed in proliferating cells, such as *TOP2A*, were downregulated.

Reconstructing the pseudotime trajectory of the three innermost cell subpopulations in goat HF

To gain a more profound understanding of HF structure, we separated the inner layer cell developmental trajectory to create pseudotime developmental trajectories for the IRS, CX, and ME groups, each enriched with various cell states. The pseudotime developmental trajectory for the ME group consisted of State 2, 3 and 4, while CX and included State 2, 3, and 5. The IRS group path comprised State 1 and 2 (Fig. 3A and B, and 4A).

To ensure the gene expression characteristics of the reconstructed trajectory were fully captured, a very small percentage of cell subpopulations from other lineages were preserved after careful consideration (Fig. 4A). Our results indicated that each branch among the three inner branches could be categorized into several subgroups, representing the origin of TAC cells and the early, intermediary, and mature stages of their differentiation process.

Next, we independently dissected the differentiation trajectory of each branch and visualized the distribution of each cell subgroup across different branches during the differentiation process (Fig. 4B, upper panel). At the beginning of differentiation, the CX, ME, and IRS branches were predominantly comprised of the TAC group. Subsequently, each branch progressed through the cell population characteristic of the early differentiation stage and proceeded to the mature stage. Interestingly, a small CX1 cell group segment appeared compatible with both ME and IRS, which might relate to their structural sandwich positioning between IRS and ME.

To further examine the gene expression features in the CX, ME, and IRS branches, we identified the differential genes in different branches using Monocle. We found that these genes were effectively divided into four clusters with different expression patterns. In the downregulated module of these three branches, TAC cell subpopulation-specific genes related to cell cycle and mitosis, such as *TOP2A*, *DCN*, *CENPW*, *CENPF*, were significantly downregulated (Fig. 4B, Table S2). By independently examining the CX branch, cluster 1 and 3 displayed an

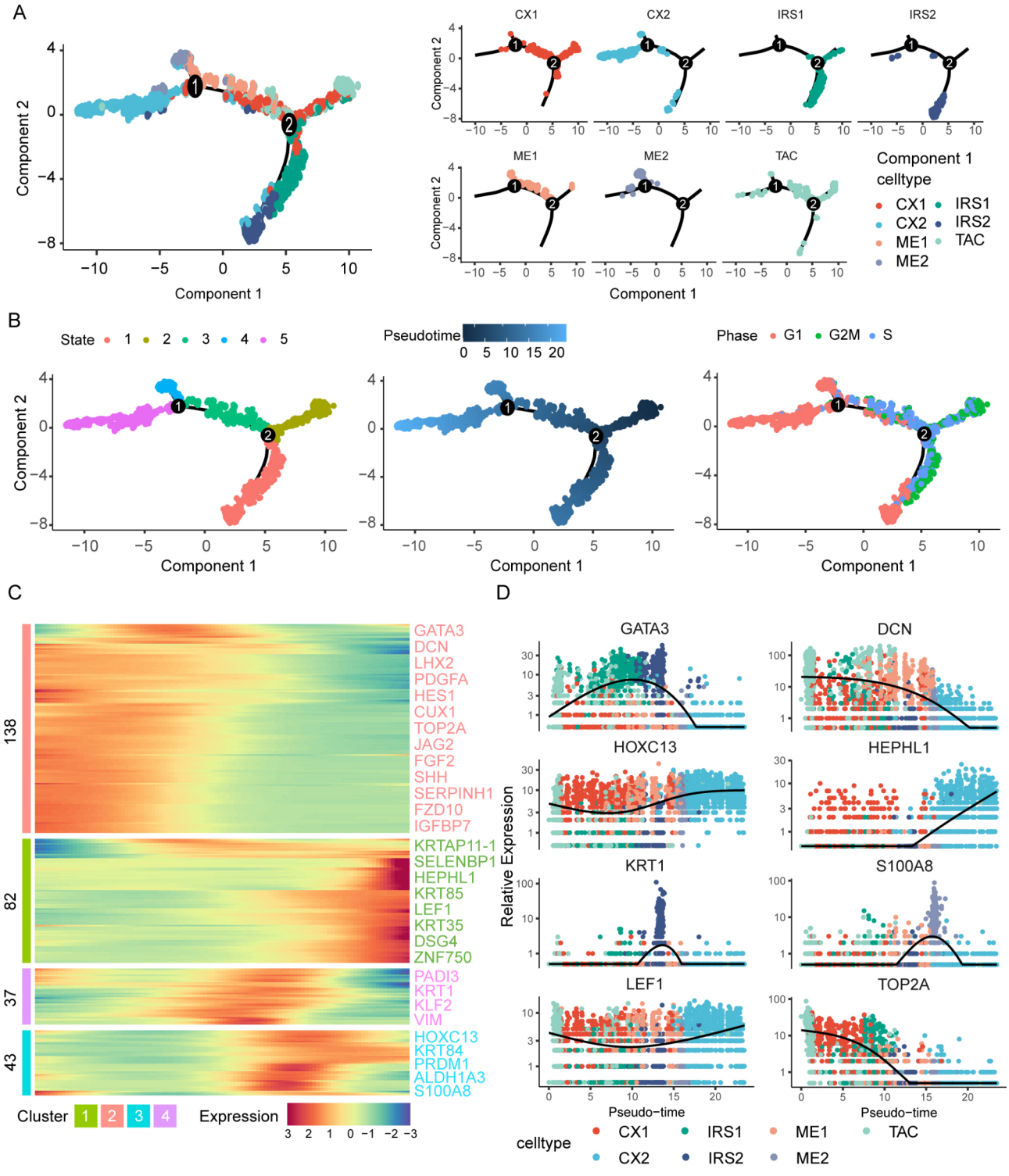

Fig. 3 Pseudotime developmental trajectory of inner layer hair follicle cells. **A** Pseudotime trajectory of inner hair follicle cells, colored by cell type. **B** Pseudotime trajectory of these cells, colored by State (left), Pseudotime (middle), and Cell Cycle (right). **C** Pseudotime expression heatmap during the fate commitment period of all inner layer HF cells, with four gene sets determined through k-means clustering based on expression patterns. **D** Characteristic genes from these four sets along the pseudotime trajectory, with cell coloring based on cell type as indicated in the bottom panel

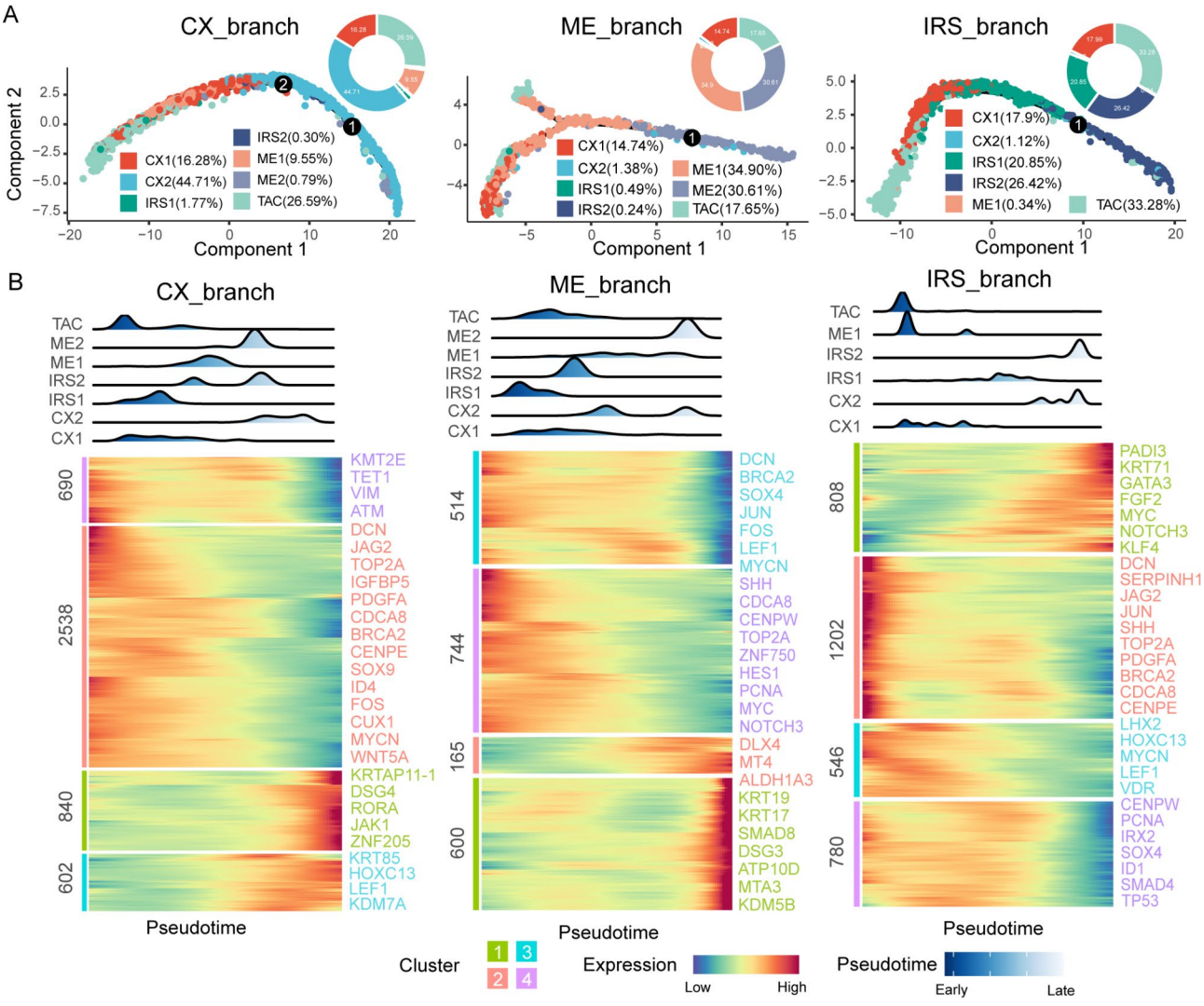

Fig. 4 Pseudotemporal trajectory of three innermost cell subgroups in HFs. **A** Reconstructed pseudotemporal developmental trajectories for three innermost cell subgroups, colored by cell subtype. Pie charts indicate the proportion of each subgroup in branches. **B** Pseudotime expression heatmap during the fate commitment period for these subgroups, with four gene sets identified by k-means clustering based on expression patterns. The upper section of the heatmap illustrates the density distribution of different cell subgroups along the pseudotemporal sequence

upregulation of CX marker genes, including *DSG4*, *LEF1*, *HEPHL1*, *SELENBP1*, and *KRT85*.

In summary, we defined three branches—IRS, CX, and ME—originating from the TAC populations. Remarkably, our study found that HF inner layer differentiation is a multi-step process. The proliferative genes of TAC subpopulation and early state populations are gradually silenced as cells exit the cell cycle. Concurrently, a specific program is induced to ensure cell differentiation along a specific lineage, ultimately achieving mature state. Especially, all branch trajectories contain cells in an intermediate state which initiates the specific intermediate molecular program (Fig. S4). We visualized 15 genes located at the beginning, middle, and end of the pseudotime trajectory to determine this cell-induced differentiation expression program (Fig. 5). The genes in the pseudotime trajectory intermediate might be associated with the identity transformation of intermediate state cells from proliferation state to the final stage of mitosis, possibly tied to the differentiation markers corresponding to distinct branches [11]. Collectively, we defined the three branches of goat HF inner layer cell subpopulations by transcription and successively uncovered the multi-step differentiation programs of various branches, yielding novel insights into the process of goat hair follicle differentiation.

Gene characteristics of three goat HF inner lineages branch

To elucidate the gene expression characteristics in different branches, we categorized the genes into upregulated and downregulated groups based on the differential genes of the three inner layer branches, and visualized

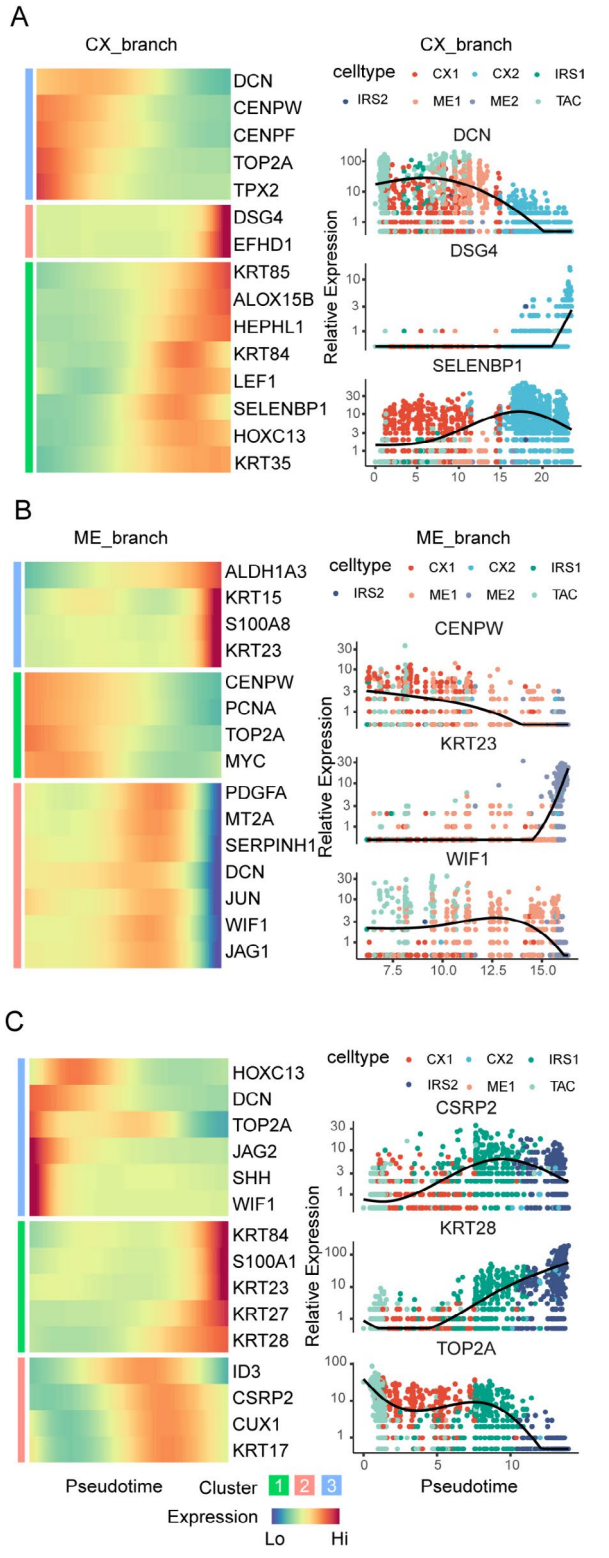

Fig. 5 Pseudotime expression heatmap of genes with varying expression patterns during inner layer differentiation. Pseudotime expression heatmap during the fate commitment period of CX (**A**), ME (**B**) and IRS (**C**) branch cells, depicting three patterns of gene expression (left) and changes in three characteristic genes along the pseudotime trajectory (right). Cell coloring is based on cell type, as shown in the top panel

using a Venn diagram. The analysis revealed that these differential genes exhibited varying specific expression levels across different branches. Notably, a higher overlap of downregulated genes was observed among the three branches (37.21% upregulated; 68.74% downregulated), potentially due to the gradual silencing of proliferating genes during development originating from a common TAC cell pool (Fig. 6A). In the upregulated genes, a substantial proportion (62.79%) are uniquely expressed in a single branch, including many lineage-specific marker genes (Tables S3-S5). In summary, the differentially expressed genes (DEGs) could be classified into three expression patterns: exclusively in one branch (Pattern 1), shared in two branches (Pattern 2), and in all three branches (Pattern 3).

To explore the expression programs of cell commitment to three different lineages, we identified the biological processes of the DEGs shared between lineages. The results indicated a strong association with cell cycle-related biological processes, such as "regulation of cell cycle process" and "cell cycle", and crucial roles in HF formation, including "epidermis development" and "epithelial morphogenesis" (Fig. 6B), linking to early differentiation stage transitions. Additionally, the involvement of TGF-β signaling, known for its regulatory role in hair follicle growth cycle [19, 20], and the "cellular response to growth factor stimulus" were also significantly enriched (Table S6). The common DEGs between branches, pertaining to intercellular communication, were further categorized and analyzed. For the DEGs in Pattern 3, a significant enrichment was observed in pathways such as "mitotic cell cycle" and "DNA metabolic process", indicating a robust proliferation and differentiation state in TAC cell subgroups during hair follicle development, which represented the starting state of progenitor cells committing to three distinct lineages (Fig. S5A). Conversely, Pattern 2 upregulated genes showed the enrichment in "epidermis development" and "keratinocyte differentiation", with notable presence of "autophagy" and "fatty acid metabolism processes", indicating the early state of progenitor cells committing to three distinct lineages (Figs. S5B-D). Interestingly, Wnt signaling, crucial in hair growth [21], showed downregulation in some branches, hinting at the formation of specific cell identities and a reduction in early transitional state characteristics (Fig. S5C). CellChat analysis further confirmed that these inner layer cell groups interacted closely during HF development (Fig. 6C and E and S6). These results enhanced our understanding on the role of intercellular communication in hair follicle inner layer cell development and the traits of inter-branch compatible genes.

To advance our knowledge of lineage-specific gene characteristics and obtain deterministic cell fate and their lineage-related differentiation markers, we conducted

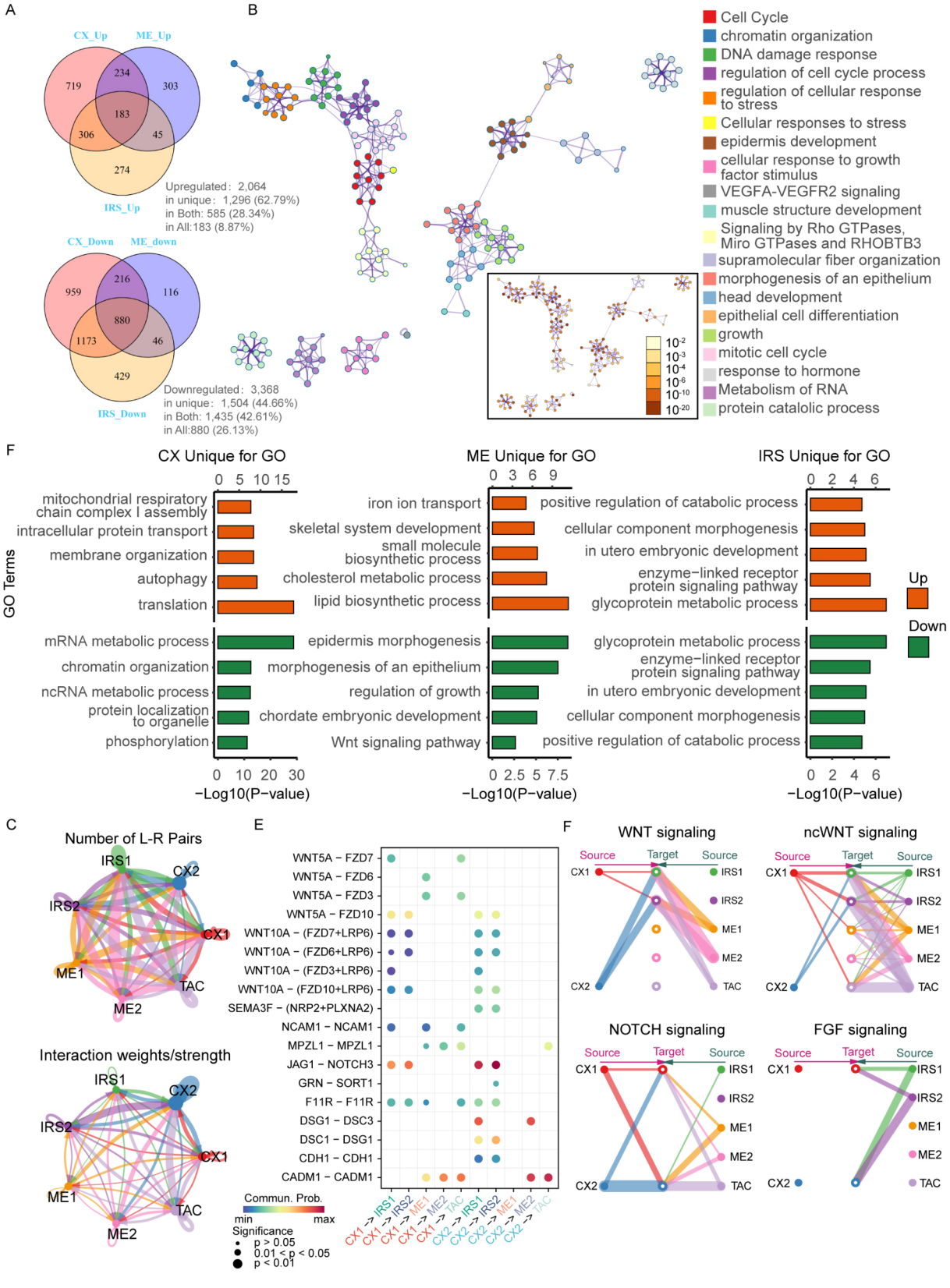

Fig. 6 (See legend on next page.)

(See figure on previous page.)

Fig. 6 Enrichment analysis of differential genes across branches and cell communication among different cell types. **A** Venn diagram representing upregulated and downregulated genes between branches, with an explanatory text below detailing the differential gene expression patterns. **B** Terms associated with differential genes shared between two branches, with the right side providing a detailed description of the involved processes. **C** GO enrichment analysis for unique differential genes in three inner layer branches, displayed in bar graphs and colored by upregulation or downregulation. **D** Illustration of cell communication among different cell types, with line thickness indicating the number and strength of receptor interactions. **E** Dot plot depicting communication between CX cells (CX1 and CX2) and other cell types, with dot size indicating significance and color representing interaction strength. **F** Diagram illustrating receptor interactions between CX cells (CX1 and CX2) and other cell types across various pathways

Gene Ontology (GO) enrichment analysis on Pattern 1 genes. The result revealed distinct enrichment patterns: "mitochondrial respiratory chain complex I assembly" and "autophagy" in CX branch differential genes, "iron ion transport" in the ME branch, and "cellular component morphogenesis" in the IRS branch (Fig. 6F). These findings underscored the diversity in biological processes influencing differentiation and emphasized the importance of intercellular communication in HF morphogenesis, especially in lineage-specific commitment processes.

Identification of lineage-specific transcription factors

To elucidate the molecular basis of lineage-specific genes, we identified transcription factors with lineage-associated expression (Fig. 7). Our analysis was restricted to the top 5% of significantly differentially expressed genes, leading to the identification of 85 lineage-specific upregulated and 315 downregulated transcription factors (Fig. 7A, S6A). To increase the reliability, we further selected the transcription factors consistently present in the top 5% of significantly different genes across the three HF inner layer branches. This approach yielded significant lineage-associated transcription factors for subsequent analysis (Fig. 7B, S6B, and Table S7). Our results identified four CX branch-specific transcription factors: LEF1, ENSCHIG00000018361 (ID2), NFE2L3, and ZNF205; ME branch-specific factors BNC1, ENSCHIG00000017707 (FOXP1), PRDM1; IRS branch-specific factors ATF3, GATA3, ID3, and others. Co-expression was observed in certain branches, with HOXC13 and ENSCHIG00000012405 (PHB1) in CX and ME branches, and ZNF750, KLF3 in CX and IRS branches, for instance (Fig. 7B). Previous studies corroborating our findings indicated that LEF1 [22] and HOXC13 [23] were critical in hair lineage differentiation during hair follicle growth, while GATA3 [14] and CUX1 [24] were vital in IRS lineage differentiation, further validating our results.

Next, we identified branch-specific keratin gene expression (Fig. 7C). Distinct keratin genes were noted for each branch: *KRT33A*, *KRT35*, and others for the CX branch; *KRT5*, *KRT15*, and *KRT19* for the ME branch; and *KRT1*, *KRT25*, and others for the IRS branch (Fig. 7D). Our findings revealed heterogeneity in keratin gene expression, with specific types like acidic type I hair keratins in the CX branch and epithelial keratins in the ME branch, demonstrating distinct differentiation stages in HF maturation.

Further analysis on the identified transcription factors involved GO enrichment analysis and exploration of potential biological processes using the STRING database. For example, the CX branch-specific transcription factor LEF1 was linked to the process of response to growth factor and epithelial morphogenesis. Similarly, the IRS branch-specific transcription factor GATA3, alongside ME branch-specific transcription factors of PRDM1 and FOXP1, was involved in the processes such as epithelial cell differentiation.

Additionally, we examined the target genes regulated by these transcription factors using the GTRD database, followed by a comparative analysis with branch-specific differential genes. This led to the discovery that the target gene of LEF1, primarily in the CX branch, were enriched in the processes of fatty acid catabolism and autophagy. In contrast, the IRS branch-specific transcription factors, including ID3, MYC, and GATA3, also influenced the processes such as the MAPK cascade and keratinocyte differentiation. Intriguingly, the target genes of ME branch-specific transcription factors e PRDM1 and FOXP1 were enriched in intracellular iron ion homeostasis term, pointing to a unique aspect of ferroptosis in HF development, further supported by Kyoto Encyclopedia of Genes and Genomes (KEGG) analysis results. Spatial localization studies further delineated the expression patterns of these lineage-specific transcription factors (Fig. 8A and C).

In summary, through scRNA-seq, we pinpointed the crucial lineage-specific transcription factors and keratin genes in the inner layers of HF. Concentrating on these transcription factors, we uncovered the potential regulatory mechanisms that drived specific lineage differentiation programs and determined the spatial localization of some factors. This study notably enhanced our understanding on lineage-specific transcription factors in the biological processes such as ferroptosis, offering novel insights into the morphogenesis of Shaanbei white cashmere goat hair follicles.

Discussion

The complex structure of hair follicles, diverse cell types, and asynchronous development of HF types presented significant challenges in understanding their early developmental processes. In our study, we leveraged

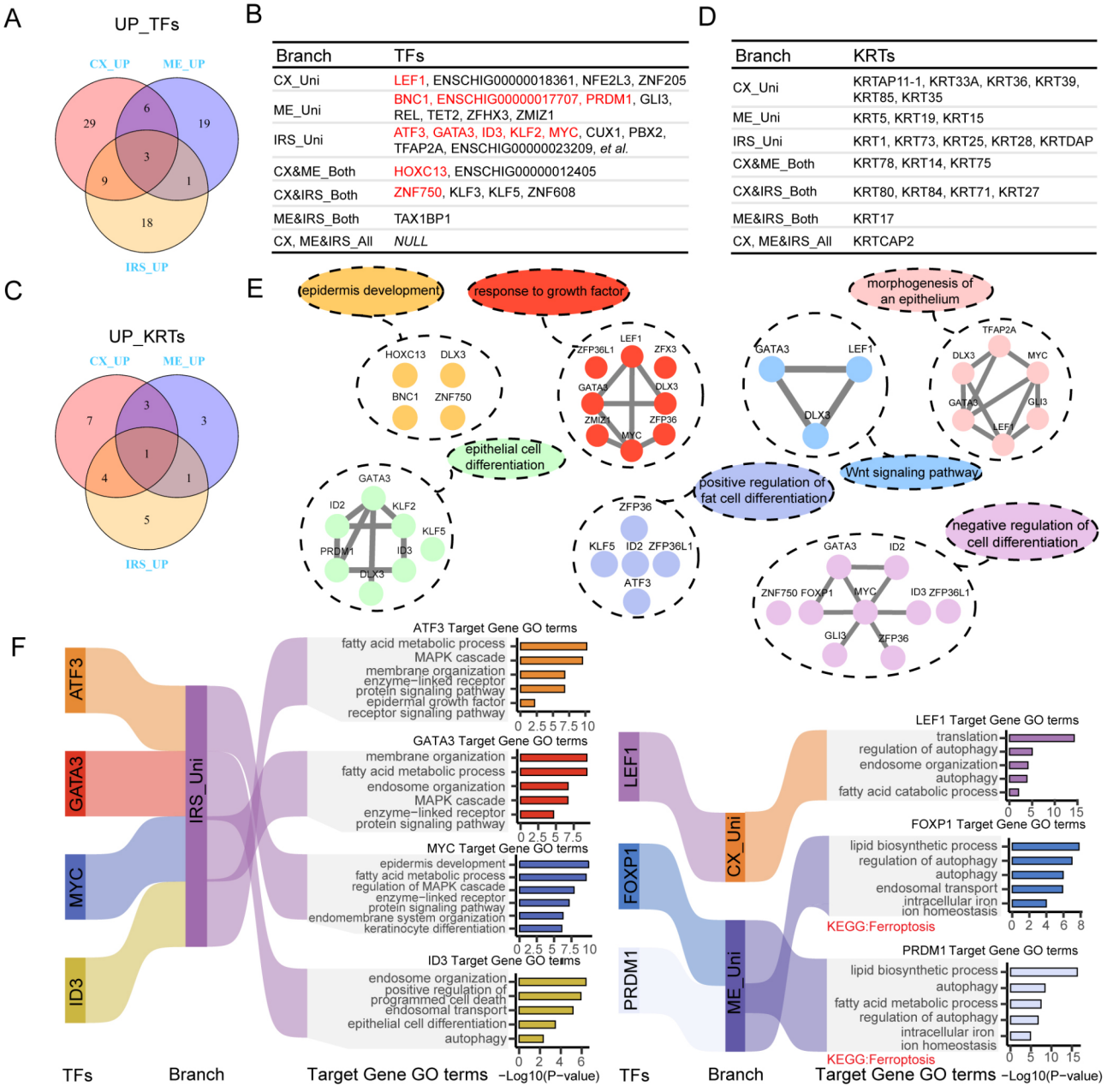

Fig. 7 Molecular characteristics of the inner layer cell fate specialization process. **A**: Venn diagram of upregulated transcription factor genes. **B** Transcription factor genes significantly upregulated in specific branches and cell types. **C** Venn diagram of upregulated keratin genes. **D** Keratin genes significantly upregulated in specific branches and cell types. **E** GO processes associated with significantly upregulated transcription factor genes in branches and cell types. **F** GO and KEGG pathways involving upregulated transcription factor target genes

scRNA-seq technology to investigate the cytodifferentiation during cashmere goat HF morphogenesis. We categorized cell types based on spatial structure characteristics, particularly in CX, ME, and IRS cell populations, thereby facilitating the construction of a detailed cellular atlas for the inner layers of cashmere goat hair follicles. Through meticulous analysis of these newly delineated cell subgroups, our research delineated the differentiation pathways within the inner layers, identifying seven distinct subgroups, and systematically established the developmental trajectories for three branches, enriched our understanding of cellular identity determination in these structures.

Mature hair follicles predominantly comprised HS and IRS [17, 18, 25], as demonstrated by our results. Focusing on these populations facilitated a deeper understanding of their ultimate developmental stages during embryonic period and provided insights into the transcriptional

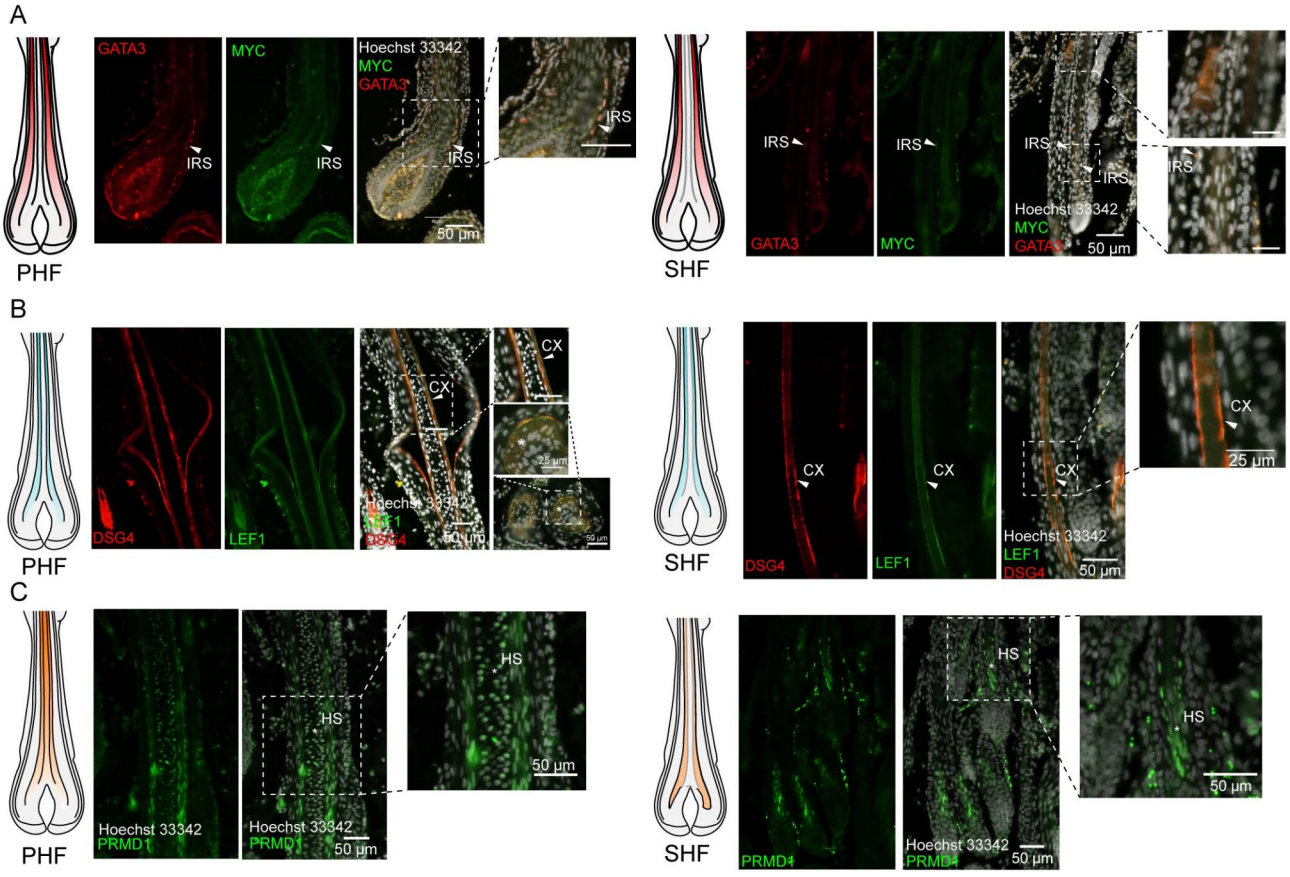

Fig. 8 Spatial localization of mature genes. Spatial localization of uniquely upregulated transcription factors (or proteins) in the IRS (**A**), CX (**B**) and ME (**C**) populations of primary and secondary hair follicles. Arrows and asterisks denoted TFs (or proteins) positive cells in two distinct hair follicle types. Scale bars, 25 μm and 50 μm

dynamics of cytodifferentiation stages. Our data revealed significant heterogeneity in HF inner layer cells and forming two distinct subgroup states due to the asynchronous nature of development: early state populations co-expressing lineage-specific and proliferative markers, and a mature cell population with unique identity features.

The study further established a topological transcriptional landscape initiating from TAC cells and branching toward IRS, CX, and ME early state subgroups with proliferative characteristics, eventually culminating in mature state populations. Consistent with the gene expression trends observed in other mammalian organ development [26], early state subpopulations displayed stronger correlations among themselves due to their derivation from common progenitor cells. Subsequently, the different mature branches became more differentiated and exhibited their own characteristics.

Significantly, this study underscored the correlation between cell fate within hair follicles and tissue position [13, 27, 28], constructing pseudotime developmental trajectories to highlight cell fate specialization during intrauterine HF morphogenesis. Notably, the CX1 subgroup emerged as a pivotal contributor to the development of both IRS and ME branches, underscoring the interconnected nature of cell differentiation across different branches, influenced by shared transcription factors [11]. For example, *Grhl1*, active in IFE differentiation, regulates IRS, CX and ME branches [11, 28]. In the ME branch, a unique division of TAC cells into two groups at the branch onset was observed (Fig. 4A), differing from the findings in mice [7, 10]. This phenomenon might due to the presence of two different hair follicle types originating from different progenitor cells in cashmere goats. The f bifurcation of the ME branch (which produces non-myelinated fibers) in the pseudotime developmental trajectory supported this idea, as suggested by Ge et al., [7]. The studies in mice also supported this hypothesis, such as the correlation between HS matrix progenitor cells (C2a-C2c) the ME1 group, which demonstrated medullary marker expression in the germinative layer [11, 28]. Additionally, our study revealed that in the early stages of branch differentiation, the CX1, ME1, and IRS1 groups occupied a central position in the differentiation trajectory. Genes like *SELENBP1*, *WIF1*, and *CSPR2* were highly expressed in these intermediate states. *SELENBP1*

was associated with goat hair growth [29], and *WIF1*, as a Wnt/β-catenin signaling pathway inhibitor, played a critical role in HF development [30, 31]. These genes might be pivotal in the transition from the proliferative to the post-mitotic stages and could be linked to markers specific to different branches.

Detailed analysis of gene expression overlap across the three differentiation trajectories demonstrated the substantial sharing of DEGs among the CX branch, ME and IRS branches, consistent with their spatial localization and location relationships in HF. Additionally, this study identified hub branch-specific down- and up-regulated genes, performing GO enrichment analysis which revealed pathways related to autophagy, Wnt signaling, and metal ion transport. These findings suggested the novel roles in ME branch specialization, hinting at the potential involvement of a nonapoptotic and iron-dependent form of cell death in ME specialization process [32]. CellChat analysis further confirmed the close interaction among the inner layer cell groups during development, suggesting a coordinated network rather than isolated pathways. Specific keratin genes expressed in different branches might influence cashmere goat hair quality. We also identified the transcription factors unique to each branch, potentially guiding differentiation direction. Transcription factors exclusively expressed in one branch included *GATA3* [14] and *CUX1* [24], known for their roles in IRS lineage differentiation, while the factors such as *HOXC13* [23], involved in hair lineage differentiation, expressed in multiple branches. Spatial location revealed that these transcription factors uniquely altered in certain branches, were not exclusively expressed in specific inner layer groups. This aligned with the existing knowledge, suggesting that hair follicle inner layer cell differentiation was a multi-step process [11]. We focused on the transcription factors uniquely up-regulated in specific branches, identifying their target genes via the GTRD database and confirming their up-regulation in respective branches. By investigating these target genes, we noted an intriguing pattern: autophagy [33, 34], essential for early hair growth, appeared to be influenced by the target genes of transcription factors uniquely up-regulated in the ME branch. These genes seemed to be involved in both autophagy and ferroptosis processes, particularly *GPX4*, which is crucial in preventing ferroptosis by eliminating phospholipid hydroperoxides [35–37]. Unfortunately, our data didn't fully clarify their interrelation. In conclusion, by analyzing the differential expression genes in the three differentiation trajectories, our study shed light on the regulatory mechanisms of HF morphogenesis and development during the cytodifferentiation stage, uncovering novel findings in cashmere goats and contributing valuable insights for breeding programs focused on cashmere traits.

Conclusion

Our scRNA-seq study elucidated the intricate molecular mechanisms driving HF morphogenesis in Shaanbei white cashmere goat. Identifying nine distinct cell populations, including seven subpopulations belonging to three primary inner layer lineages, underscored the remarkable cellular heterogeneity and the crucial roles of lineage-specific TFs such as GATA3, LEF1, and PRDM1. These TFs, along with their target genes and keratin genes, played pivotal roles in HF development. The detailed analysis of cytodifferentiation stage, essential for the formation of the HS and IRS, provided significant insights with profound implications for the quality of cashmere. Additionally, the delineation of key lineage-specific transcription factors laid the foundation for the innovative genetic and breeding strategies to improve fiber quality. This study not only deepened our understanding of HF biology in cashmere goats but also provided strategic insights for advancing the cashmere industry.

Materials and methods

Sample collection and scRNA-seq

Sequencing sample preparation followed the methodology outlined in a previous study, and three fetuses ($n=3$) from three pregnant female goats were processed for scRNA-seq dataset [7]. Experimental preparation, starting at E120, involved isolating skin tissues from the dorsolateral skin of each fetus. Goats were anesthetized with 0.3 mg/kg of xylazine hydrochloride (Catalog No. 070011582, Huamu Animal Health Products Co., Ltd., Hangzhou, China) administered intravenously, and the fetuses were delivered via caesarean section. Following anesthesia, the female goats received continuous monitoring and appropriate postoperative care. Both female goats and fetuses remained unconscious throughout the procedure. After cutting the umbilical cord, the fetuses were euthanized due to hypoxia while unconscious, in accordance with the AVMA Guidelines for the Euthanasia of Animals: 2020 Edition, as detailed in previous study [38]. The bodies of fetuses were subsequently frozen and transported to a designated site for biosecurity processing. Ethical approval for the sample collection procedures was granted by the Northwest A&F University Animal Care Committee (Permit Number: NWAFAC1019). All operations and experimental procedures adhered to the national standard of the People's Republic of China, "Laboratory animal-Guideline for ethical review of animal welfare" (GB/T 35892–2018) and the "Guide for the Care and Use of Laboratory Animals: Eighth Edition" [39], with meticulous measures taken to minimize invasiveness.

The tissues were immersed in ice-cold DMEM/F12 media (Catalog No. C11330500BT, Gibco, Beijing,

China), supplemented with 50 U/ml penicillin and 50 mg/ml streptomycin (Catalog No. SV30010, HyClone, Logan, UT). Skin tissue samples slated for scRNA-seq received treatment consistent with our prior report, whereas the remaining samples for immunohistochemistry were fixed overnight at 4 °C with 4% paraformaldehyde (PFA, Biosharp, BL539A, Hefei, China).

The single-cell system of the 10× Genomics platform was employed for the generation of gel bead emulsions (GEMs). The 10× Genomics Chromium Single-Cell 3' library and GelBead Kit v3 (Illumina, San Diego, CA) were utilized for reverse transcription, barcode assignment, and library construction, following the manufacturer's protocol. Paired-end sequencing was conducted using an Illumina HiSeq X Ten sequenator (Illumina, San Diego, CA) provided by Novogene Bioinformatics Co., Ltd. (Beijing, China).

Analysis of scRNA-seq data

Initial data processing and quality control

The raw 10× sequencing data underwent processing to generate a matrix utilizing the standard 10× CellRanger pipeline. In brief, the base call files were in fastq format and were aligned to the Capra hircus ARS1 reference genome. Subsequent steps involved the counting of unique molecular identifiers (nUMI) and barcodes, leading to the construction of nUMI count matrices. Fig. S1A offers a comprehensive summary of cells captured in the sample, encompassing metrics such as the total number of captured cells, the median gene count, and the count of individual genes. Then, the subsequent bioinformatics analysis was conducted using the Seurat package (v.4.3.0) [40] within the R environment. Initial quality control involved assessing parameters related to transcript characteristics, such as the proportion of mitochondrial genes in each sample. Simultaneously, low-quality cells were excluded from the samples, specifically those with gene expression below 200 cells and genes expressed less than 3 cells. Additional filtering criteria were applied to cells, necessitating > 1,500 nGene but < 4,000, nUMI > 200 but < 50,000, and a proportion of mitochondrial genes (percent.mt) < 10% (Fig. S1B). Relationships between the percentage of mitochondrial genes and mRNA reads, as well as the relationship between the number of mRNAs and mRNA reads, were concurrently detected and visualized (Fig. S1C).

Visualization and clustering

Furthermore, the *FindVariableFeatures* function implemented in Seurat package identified a highly variable gene set (Fig. S1D). Additionally, the DoubletFinder package (v.2.0.3) [41] default process was utilized to remove the potential "Doublets" (where a double cell was considered as one cell in sequencing). Ultimately, 4,995 "Singlets" were retained (Figs. S1E and S1F). Simultaneously, the use of "Anchors" a mechanism transforming a dataset into a shared space by identifying cell-pair correspondences between individual cells in the dataset, facilitated data integration [42]. The functions *RunUMAP*, *FindClusters* and *FindNeighbors* were executed to generate cell clusters. Following experiments and adjustments, the parameter resolution was set to 0.8 for clustering all cells and 0.5 for clustering inner layer cells, ensuring optimal clustering results. Subsequently, the *FindAllMarkers* function was employed to compute marker genes specific to each cluster, facilitating the identification of cell types in the sample. Moreover, Seurat provided functionalities like *Dotplot*, *FeaturePlot*, and *DoHeatmap* for visualizing the expression of specific genes.

Prediction of cell cycle stage

Within hair follicles, heterogeneity in cell cycle phases contributed to a substantial number of transcriptome mutations [11]. To precisely examine the potential relationship between each cell group and cell cycle, we employed the *CellCycleScoring* function implemented in the Seurat package to predict cell cycle stages. Cells with both G1/S and G2/M cycle scores below 2 were deemed aperiodic; otherwise, we categorized them as proliferating. The prediction of cell cycle phase for each cell cluster is shown in Fig. S1G and 3 C.

Analysis of pesudotime trajectory with Monocle

Monocle (v2.28.0) [43] R package was utilized based on the genes identified by the Seurat package with high variable. Single-cell pseudotime trajectories were generated using the functions *reduceDimension* and *orderCells*. Upon obtaining the pseudotime trajectory tree, the distribution of states became visually apparent, allowing for easy examination of the transcriptional patterns of cells in each "State". The function *plot_genes_branched_heatmap* was primarily used to construct the heatmap for each gene set, and the *plot_genes_in_pseudotime* function was employed to visualize the pseudotime trajectory of branch-specific genes, providing insights for determining cell developmental fate.

Establishment of TF-Target gene network

To identify potentially altered TFs and compile a list specific to goats, we employed the curated AnimalTFDB 4.0 database (http://bioinfo.life.hust.edu.cn/AnimalTFDB4/) by Shen et al. [44]. Subsequently, we identified the target genes of these TFs using the GTRD database (http://gtrd.biouml.org/), proposed by Kolmykov et al. [45]. While the GTRD database primarily contained targeting relationships for human TFs, we posited that the conservation of homologous genes/proteins extends to goats, allowing the application of these targeting relationships.

In constructing TFs-Target gene regulatory networks, at least one transcription factor was considered for each unique branch.

Analysis of functional enrichment

To comprehensively analyze the DEGs in single cell data, the effective and efficient tool Metascape (http://metascape.org/) [46] was used. The diligent maintenance by Metascape developers ensured the database's timely updates, and this study employed Metascape to retrieve the latest GO and KEGG analyses. Additionally, we utilized the STRING database (https://string-db.org/) [47], a resource systematically gathering and integrating protein-protein interactions, encompassing both physical interactions and functional associations, to construct protein-protein association networks.

Immunofluorescence of skin tissues

Skin tissues were processed and embedded in paraffin following standard histological procedures. A Leica Slicer (RM2255, Heidelberger, Germany) was employed for paraffin sectioning with a thickness of 5 μm, followed by rehydration using a gradient ethanol series. Antigen recovery of the sections occurred at room temperature following degeneration in a 0.01 mol/L sodium citrate solution at 96 °C for 10 min. Subsequently, slides were blocked with BDT (TBS containing 3% bovine serum albumin and 10% normal goat serum) for 30 min, followed by overnight incubation at 4 °C with the primary antibodies diluted in BDT. After primary antibodies incubation, slides were left at room temperature for approximately 30 min, rinsed with TBST three times, and then incubated with corresponding secondary antibodies at 37 °C for 45 min. Nuclei were labeled by pretreating the slides with 1 μg/mL Hoechst 33,342 (Beyotime, C1022, Shanghai, China) for 5 min. Observations were carried out using a IX73 microscope (Olympus, Tokyo, Japan). All antibodies are listed in table S1.

Abbreviations

HF	Hair Follicle
SHF	Secondary Hair Follicle
DPC	Dermal Papilla Cell
scRNA-seq	Single-cell RNA Sequencing
TGF-β	Transforming Growth Factor Beta
CX	Cortex/Cuticle
TAC	Transient Amplifying Cells
ORS	Out Root Sheath
IRS	Inner Root Sheath
ME	Medulla
GO	Gene Ontology
KEGG	Kyoto Encyclopedia of Genes and Genomes
DEG(s)	Differentially Expressed Gene(s)
GTRD	The Gene Transcription Regulation Database

Supplementary Information

The online version contains supplementary material available at https://doi.org/10.1186/s12864-024-10820-2.

Supplementary Material 1
Supplementary Material 2
Supplementary Material 3
Supplementary Material 4
Supplementary Material 5
Supplementary Material 6
Supplementary Material 7
Supplementary Material 8
Supplementary Material 9
Supplementary Material 10
Supplementary Material 11
Supplementary Material 12
Supplementary Material 13
Supplementary Material 14

Acknowledgements

We thank the High-Performance Computing Center (HPC) of Northwest A&F University (NWAFU) for providing computing resources.

Author contributions

ML: Methodology, Formal analysis, Visualization, Software, Conceptualization, Writing - original draft, Writing - review & editing. XH: Methodology, Formal analysis, Visualization. ZC: Software, Writing - review & editing. JD: Methodology, Visualization, Software. XW1: Methodology, Formal analysis, Visualization. NW: Formal analysis, Validation, Visualization. TZ: Formal analysis, Visualization. ZZ: Formal analysis, Visualization. XW2: Conceptualization, Supervision, Writing - review & editing.

Funding

This study was supported by the National Natural Science Foundation of China (Grant No. U23A20226).

Data availability

The sequence data supporting the findings of this study have been deposited in the Gene Expression Omnibus (GEO) repository at the National Center for Biotechnology Information (GEO: GSE144351).

Declarations

Ethics approval and consent to participate

The Shaanbei white cashmere goats utilized in this study were obtained from the Shaanbei Cashmere Goat Engineering Technology Research Center of Shaanxi Province (Yulin, China). Ethical approval for sample collection procedures was granted by the Northwest A&F University Animal Care Committee (Permit Number: NWAFAC1019). All operations and experimental procedures adhered to the national standard of the People's Republic of China "Laboratory animal-guideline for ethical review of animal welfare" (GB/T 35892 – 2018) and the "Guide for the Care and Use of Laboratory Animals: Eighth Edition", with meticulous measures taken to minimize invasiveness.

Consent for publication

Not applicable.

Competing interests

The authors declare no competing interests.

Received: 15 May 2024 / Accepted: 20 September 2024
Published online: 15 October 2024

References

1. Waldron S, Brown C, Komarek AM. The Chinese cashmere industry: a global value chain analysis. Dev Policy Rev. 2014;32(5):589–610.
2. Nocelli C, Cappelli K, Capomaccio S, Pascucci L, Mercati F, Pazzaglia I, Mecocci S, Antonini M, Renieri C. Shedding light on cashmere goat hair follicle biology: from morphology analyses to transcriptomic landascape. BMC Genomics. 2020;21(1):458.
3. Gong G, Fan Y, Yan X, Li W, Yan X, Liu H, Zhang L, Su Y, Zhang J, Jiang W, et al. Identification of genes related to hair follicle cycle development in Inner Mongolia cashmere goat by WGCNA. Front Vet Sci. 2022;9:894380.
4. Zhang B, Chen T. Local and systemic mechanisms that control the hair follicle stem cell niche. Nat Rev Mol Cell Biol 2023.
5. Hardy MH. The secret life of the hair follicle. Trends Genet. 1992;8(2):55–61.
6. Wang Z, Wang Y, Hui T, Chen R, Xu Y, Zhang Y, Tian H, Wang W, Cong Y, Guo S, et al. Single-cell sequencing reveals differential cell types in skin tissues of Liaoning cashmere goats and key genes related potentially to the fineness of cashmere Fiber. Front Genet. 2021;12:726670.
7. Ge W, Zhang W, Zhang Y, Zheng Y, Li F, Wang S, Liu J, Tan S, Yan Z, Wang L, et al. A single-cell transcriptome atlas of cashmere goat hair follicle morphogenesis. Genom Proteom Bioinform. 2021;19(3):437–51.
8. Yang F, Li R, Zhao C, Che T, Guo J, Xie Y, Wang Z, Li J, Liu Z. Single-cell sequencing reveals the new existence form of dermal papilla cells in the hair follicle regeneration of cashmere goats. Genomics. 2022;114(2):110316.
9. Zhang Y-j, Yin J, Li C-q. Study on development of skin and hair follicle from fetal inner Mongolian arbas cashmere goats. Acta Vet Et Zootechnica Sinica. 2006;37(8):761.
10. Ge W, Tan SJ, Wang SH, Li L, Sun XF, Shen W, Wang X. Single-cell transcriptome profiling reveals dermal and epithelial cell fate decisions during embryonic hair follicle development. Theranostics. 2020;10(17):7581–98.
11. Joost S, Annusver K, Jacob T, Sun X, Dalessandri T, Sivan U, Sequeira I, Sandberg R, Kasper M. The molecular anatomy of mouse skin during hair growth and rest. Cell Stem Cell. 2020;26(3):441–e457447.
12. Hsu YC, Li L, Fuchs E. Transit-amplifying cells orchestrate stem cell activity and tissue regeneration. Cell. 2014;157(4):935–49.
13. Morita R, Sanzen N, Sasaki H, Hayashi T, Umeda M, Yoshimura M, Yamamoto T, Shibata T, Abe T, Kiyonari H, et al. Tracing the origin of hair follicle stem cells. Nature. 2021;594(7864):547–52.
14. Kaufman CK, Zhou P, Pasolli HA, Rendl M, Bolotin D, Lim KC, Dai X, Alegre ML, Fuchs E. GATA-3: an unexpected regulator of cell lineage determination in skin. Genes Dev. 2003;17(17):2108–22.
15. Detmar M, Brown LF, Schon MP, Elicker BM, Velasco P, Richard L, Fukumura D, Monsky W, Claffey KP, Jain RK. Increased microvascular density and enhanced leukocyte rolling and adhesion in the skin of VEGF transgenic mice. J Invest Dermatol. 1998;111(1):1–6.
16. Driskell RR, Giangreco A, Jensen KB, Mulder KW, Watt FM. Sox2-positive dermal papilla cells specify hair follicle type in mammalian epidermis. Development. 2009;136(16):2815–23.
17. Fuchs E. Scratching the surface of skin development. Nature. 2007;445(7130):834–42.
18. Schneider MR, Schmidt-Ullrich R, Paus R. The hair follicle as a dynamic miniorgan. Curr Biol. 2009;19(3):R132–142.
19. Oshimori N, Fuchs E. Paracrine TGF-beta signaling counterbalances BMP-mediated repression in hair follicle stem cell activation. Cell Stem Cell. 2012;10(1):63–75.
20. Plasari G, Edelmann S, Hogger F, Dusserre Y, Mermod N, Calabrese A. Nuclear factor I-C regulates TGF-beta-dependent hair follicle cycling. J Biol Chem. 2010;285(44):34115–25.
21. Tsai SY, Sennett R, Rezza A, Clavel C, Grisanti L, Zemla R, Najam S, Rendl M. Wnt/beta-catenin signaling in dermal condensates is required for hair follicle formation. Dev Biol. 2014;385(2):179–88.
22. Zhou P, Byrne C, Jacobs J, Fuchs E. Lymphoid enhancer factor 1 directs hair follicle patterning and epithelial cell fate. Genes Dev. 1995;9(6):700–13.
23. Jave-Suarez LF, Winter H, Langbein L, Rogers MA, Schweizer J. HOXC13 is involved in the regulation of human hair keratin gene expression. J Biol Chem. 2002;277(5):3718–26.
24. Ellis T, Gambardella L, Horcher M, Tschanz S, Capol J, Bertram P, Jochum W, Barrandon Y, Busslinger M. The transcriptional repressor CDP (Cutl1) is essential for epithelial cell differentiation of the lung and the hair follicle. Genes Dev. 2001;15(17):2307–19.
25. Saxena N, Mok KW, Rendl M. An updated classification of hair follicle morphogenesis. Exp Dermatol. 2019;28(4):332–44.
26. Cardoso-Moreira M, Halbert J, Valloton D, Velten B, Chen C, Shao Y, Liechti A, Ascencao K, Rummel C, Ovchinnikova S, et al. Gene expression across mammalian organ development. Nature. 2019;571(7766):505–9.
27. Xin T, Gonzalez D, Rompolas P, Greco V. Flexible fate determination ensures robust differentiation in the hair follicle. Nat Cell Biol. 2018;20(12):1361–9.
28. Yang H, Adam RC, Ge Y, Hua ZL, Fuchs E. Epithelial-mesenchymal micro-niches govern stem cell lineage choices. Cell. 2017;169(3):483–e496413.
29. Li Y, Zhou G, Zhang R, Guo J, Li C, Martin G, Chen Y, Wang X. Comparative proteomic analyses using iTRAQ-labeling provides insights into fiber diversity in sheep and goats. J Proteom. 2018;172:82–8.
30. Zhao B, Li J, Zhang X, Dai Y, Yang N, Bao Z, Chen Y, Wu X. Exosomal miRNA-181a-5p from the cells of the hair follicle dermal papilla promotes the hair follicle growth and development via the Wnt/beta-catenin signaling pathway. Int J Biol Macromol. 2022;207:110–20.
31. Manandhar S, Kabekkodu SP, Pai KSR. Aberrant canonical wnt signaling: Phytochemical based modulation. Phytomedicine. 2020;76:153243.
32. Tang D, Chen X, Kang R, Kroemer G. Ferroptosis: molecular mechanisms and health implications. Cell Res. 2021;31(2):107–25.
33. Chai M, Jiang M, Vergnes L, Fu X, de Barros SC, Doan NB, Huang W, Chu J, Jiao J, Herschman H, et al. Stimulation of hair growth by small molecules that activate autophagy. Cell Rep. 2019;27(12):3413–e34213413.
34. Yoshihara N, Ueno T, Takagi A, Oliva Trejo JA, Haruna K, Suga Y, Komatsu M, Tanaka K, Ikeda S. The significant role of autophagy in the granular layer in normal skin differentiation and hair growth. Arch Dermatol Res. 2015;307(2):159–69.
35. Yang WS, SriRamaratnam R, Welsch ME, Shimada K, Skouta R, Viswanathan VS, Cheah JH, Clemons PA, Shamji AF, Clish CB, et al. Regulation of ferroptotic cancer cell death by GPX4. Cell. 2014;156(1–2):317–31.
36. Shimada K, Skouta R, Kaplan A, Yang WS, Hayano M, Dixon SJ, Brown LM, Valenzuela CA, Wolpaw AJ, Stockwell BR. Global survey of cell death mechanisms reveals metabolic regulation of ferroptosis. Nat Chem Biol. 2016;12(7):497–503.
37. Yang L, Chen X, Yang Q, Chen J, Huang Q, Yao L, Yan D, Wu J, Zhang P, Tang D, et al. Broad spectrum deubiquitinase inhibition induces both apoptosis and ferroptosis in cancer cells. Front Oncol. 2020;10:949.
38. Wang S, Luo Z, Zhang Y, Yuan D, Ge W, Wang X. The inconsistent regulation of HOXC13 on different keratins and the regulation mechanism on HOXC13 in cashmere goat (Capra hircus). BMC Genomics. 2018;19(1):630.
39. Edition E. Guide for the care and use of laboratory animals. Washington: the national academies; 2011.
40. Hao Y, Hao S, Andersen-Nissen E, Mauck WM 3rd, Zheng S, Butler A, Lee MJ, Wilk AJ, Darby C, Zager M, et al. Integrated analysis of multimodal single-cell data. Cell. 2021;184(13):3573–e35873529.
41. McGinnis CS, Murrow LM, Gartner ZJ. DoubletFinder: doublet detection in single-cell RNA sequencing data using artificial nearest neighbors. Cell Syst. 2019;8(4):329–e337324.
42. Stuart T, Butler A, Hoffman P, Hafemeister C, Papalexi E, Mauck WM 3rd, Hao Y, Stoeckius M, Smibert P, Satija R. Comprehensive Integration of single-cell data. Cell. 2019;177(7):1888–e19021821.
43. Qiu X, Mao Q, Tang Y, Wang L, Chawla R, Pliner HA, Trapnell C. Reversed graph embedding resolves complex single-cell trajectories. Nat Methods. 2017;14(10):979–82.
44. Shen WK, Chen SY, Gan ZQ, Zhang YZ, Yue T, Chen MM, Xue Y, Hu H, Guo AY. AnimalTFDB 4.0: a comprehensive animal transcription factor database updated with variation and expression annotations. Nucleic Acids Res. 2023;51(D1):D39–45.
45. Kolmykov S, Yevshin I, Kulyashov M, Sharipov R, Kondrakhin Y, Makeev VJ, Kulakovskiy IV, Kel A, Kolpakov F. GTRD: an integrated view of transcription regulation. Nucleic Acids Res. 2021;49(D1):D104–11.
46. Zhou Y, Zhou B, Pache L, Chang M, Khodabakhshi AH, Tanaseichuk O, Benner C, Chanda SK. Metascape provides a biologist-oriented resource for the analysis of systems-level datasets. Nat Commun. 2019;10(1):1523.
47. Szklarczyk D, Kirsch R, Koutrouli M, Nastou K, Mehryary F, Hachilif R, Gable AL, Fang T, Doncheva NT, Pyysalo S, et al. The STRING database in 2023: protein-protein association networks and functional enrichment analyses for any sequenced genome of interest. Nucleic Acids Res. 2023;51(D1):D638–46.

Publisher's note